Polymer 51 (2010) 5506–5515

Contents lists available at ScienceDirect

Polymer

journal homepage: www.elsevier.com/locate/polymer

Effect of polymer/filler interactions on the structure and rheological properties of ethylene-octene copolymer/nanosilica composites

Mathieu Bailly [a], Marianna Kontopoulou [a,*], Khalil El Mabrouk [b]

[a] Department of Chemical Engineering, Queen's University, Kingston, ON, Canada K7L 3N6
[b] Institute of Nanomaterials and Nanotechnology, MAScIR (Moroccan Advanced Science, Innovation and Research Foundation), Rabat, Morocco

ARTICLE INFO

Article history:
Received 25 June 2010
Received in revised form
17 September 2010
Accepted 21 September 2010
Available online 25 September 2010

Keywords:
Nanocomposites
Fumed silica
Silane-grafted polyolefins

ABSTRACT

The microstructure and rheology of melt compounded ethylene-octene copolymer (EOC) nanocomposites, containing different types of functionalized matrices and nanosilica particles, were investigated. The EOC matrix was functionalized via silane grafting, using monofunctional (vinyltriethylsilane-VTES) or bifunctional (vinyltriethoxysilane VTEOS) silane agents, to prepare EOC-g-VTES and EOC-g-VTEOS respectively. Two different types of silica were used, unmodified (SiO_2), or modified with octylsilane (oct-SiO_2). Depending on the matrix/filler combination, different types of polymer/filler interactions were present in these composites. The formation of covalent bonds between the VTEOS functionality and the hydroxyl groups present at the surface of the particles, generated strong polymer/filler interactions, resulting in improved filler dispersion. The presence of polymer/filler interactions was confirmed by bound polymer measurements. TEM micrographs revealed a fractal-like composite structure, which agreed with the exponents determined through small angle oscillatory shear rheometry (SAOS). Rheological properties in the melt state revealed significant differences, depending on the types of matrix and filler used. Time-sweep experiments showed pronounced time-dependence indicative of a tendency toward aggregation for the EOC-g-VTES-based composites. On the contrary, strong polymer/filler interactions between EOC-g-VTEOS and oct-SiO_2 resulted in a stable response. During strain-sweep experiments the EOC-g-VTEOS-based composites exhibited a higher critical strain for the onset of non-linearity, indicative of stronger adhesion between the fillers and the matrix. DMA measurements showed that more energy is dissipated during the glass transition in the composites with enhanced polymer/filler interactions.

1. Introduction

Colloidal silica suspensions have been used extensively in applications involving paints, foodstuffs, as well as in emerging technologies such as photonics and microelectronics, due to their function as thickening and thixotropic agents in low molecular weight solvents [1,2]. Fumed and precipitated silica particles have also successfully served as reinforcing agents for rubbers [3] and more recently for thermoplastic matrices [4].

The unique properties of silica nanoparticles arise from their surface chemistry characterized by the presence of silanol groups. When dispersed in a liquid medium, aggregates of primary particles interact via hydrogen bonding, giving rise to larger flocculated structures called flocs. As the concentration of particles in solution increases, a sol–gel transition is eventually reached, characterized by the formation of a three-dimensional network and the appearance of a gel-like structure. This specific arrangement of particles in a space-filling network can be described by a fractal geometry [5,6]. The gelation process depends strongly on several variables, such as the volume fraction of nanoparticles, the type of particles used (hydrophilic vs. hydrophobic) and the nature of the suspending medium (polar vs. non-polar). As a result, a wide range of materials can be prepared, from low viscosity sols to elastic gels [2].

The steady-shear rheology of silica-containing suspensions is characterized by pronounced shear thickening and is influenced by the transient disruption and buildup of the filler network [1,7]. Scaling relations obtained through linear and non-linear viscoelasticity measurements [2,8–10] have been associated to the fractal dimensions of the flocculated silica structures, as obtained by image analysis or light-scattering [6,11].

Studies on polymeric matrices have mostly focused on elastomer technology. Using thermodynamic arguments, Wang et al. showed that in filled rubber compounds differences in the surface energy between filler and polymer cause flocculation of the filler aggregates in a manner similar to that observed in colloidal systems

* Corresponding author. Tel.: +1 613 533 3079; fax: +1 613 533 6637.
E-mail address: marianna.kontopoulou@chee.queensu.ca (M. Kontopoulou).

0032-3861/$ – see front matter © 2010 Elsevier Ltd. All rights reserved.
doi:10.1016/j.polymer.2010.09.051

[12]. Experimental evidence in elastomers points to the concept of a network structure that refers to a space-filling configuration of kinetically aggregated filler clusters [13]. A structure comprised of rigid filler particles with fractal structure has also been suggested by Huber and Vilgis [14].

The rheological properties of polymer composites are related to the work of adhesion between the filler surface and the polymer matrix [15]. Therefore a lot of attention has been paid on the rheology of composites containing high molecular weight suspending media, being either polymers in the melt state or polymer solutions. Dramatic increases in the storage moduli at low frequencies, leading to the appearance of a secondary plateau or a "solid-like behaviour" and a drop of the storage modulus upon increasing strain, also known as the "Payne effect" are commonly observed [16]. The scaling relations governing these composites are similar to those reported for suspensions [16].

Similarly to the gelation process, the rheological response of polymer-based composites is influenced substantially by the extent of polymer/filler interactions, which in turn depend upon the surface treatment of the particles, and the nature of the polymeric matrix. Strong polymer/filler interactions may occur between hydrophilic silica particles with a high specific surface area and a polar matrix [17], or when bifunctional coupling agents are used to modify nanoparticles in order to form covalent bonds with the functional groups present in the polymer matrix [18,19]. These interactions may lead to the formation of an immobilized layer or "bound" polymer surrounding the filler particles. The presence of bound polymer has been frequently evoked in elastomer technology to explain the enhanced hydrodynamic effect, leading to an increase in the modulus when filler particles are added in elastomeric matrices [12]. The presence of chemical bonds between the matrix and the fillers is crucial to achieve improved mechanical properties of the resulting composites [20–22], however the influence of chemical bonds on the rheological properties of the composites is still unclear.

In this work we have used an ethylene-octene copolymer (EOC) matrix functionalized with a reactive and a non-reactive silane, the former of which forms chemical bonds with the surface silanol groups of the nanosilica particles. Based on detailed rheological characterization and imaging, we investigate the influence of the presence of chemical bonds on the structure of the composites and their rheological response.

2. Experimental

2.1. Materials

The ethylene-octene copolymer (EOC), trade name Engage 8130, density 0.864 g cm^{-3}, MFI 13 g/10 min at 190 °C, copolymer content 42 wt%, was obtained from Dow Chemical. The melting and crystallization temperatures of this polymer, as measured by DSC are 67.1 °C and 40 °C respectively, and the degree of crystallinity is 3.7%. Vinyltriethoxysilane (VTEOS, 97%, Aldrich Chemical Company Inc.), vinyltriethylsilane (VTES, 98%, Sigma–Aldrich) and dicumyl peroxide (DCP, 98%, Sigma–Aldrich) were used as received.

Two different types of silica with an average particle size of 12 nm were supplied by Evonik Industries (formerly Degussa Corp.): A hydrophilic fumed silica Aerosil® 200 with a specific surface area (SSA) of 200 ± 25 m^2/g, and a hydrophobic surface modified nanosilica Aerosil® R805 modified with octylsilane (oct-SiO_2) having a SSA of 150 ± 25 m^2/g. Detailed characterization of the fillers, including TGA and FT-IR characterization can be found in our previous work [23].

2.2. Grafting procedure and composite preparation

EOC pellets were premixed with 0.1 wt% of DCP and 2 wt% of VTEOS or VTES in a Haake PolyLab rheometer equipped with a Rheomix 610p mixing chamber and roller rotors at 80 °C for 10 min at 60 rpm. The material was subsequently removed and reintroduced in the mixer at 180 °C and 60 rpm to accomplish the grafting reaction and obtain EOC-g-VTEOS or EOC-g-VTES, depending on the type of monomer used. The grafting mechanism has been described elsewhere [24]. After completion of the grafting reaction (about 5 min) the fillers were added and compounded for a total of 12 min, according to the compositions given in Table 1. The weight fractions shown in Table 1 were converted to volume fractions by using a density of 2.2 g cm^{-3} for the nanosilica, 0.864 g cm^{-3} for the solid polymer and 0.760 g cm^{-3} for the molten polymer [25].

It should be noted that the calculated volume fractions represent the volume that the fumed silica would occupy if it were in a compacted state. The open structure of the fumed silica however renders the effective volume fraction significantly larger than this calculated value [2]. Therefore due to the extremely low bulk density of the nanosilica, a 12 wt% composite is already highly filled. We have not attempted to study composites with higher filler loadings due to difficulties in melt compounding higher amounts of silica. Additionally the contents of interest from a practical standpoint are well below 12 wt%.

2.3. Characterization of functionalized EOC

FT-IR spectra were obtained using a Nicolet Avatar 360 FT-IR ESP instrument. Graft contents were calculated from FT-IR integrations of the absorbance of the silanes relative to an internal standard region originating from the plain matrix. Purification of the polymer prior to FT-IR evaluations was carried out by dissolution in hot refluxing xylene, precipitation from acetone, and drying under vacuum at 60 °C overnight.

A calibration curve for the determination of the graft content was obtained by using known mixtures of the polymer matrix and the VTE(O)S monomers as standards. Based on this method, the amount of VTE(O)S grafted onto the EOC matrix was estimated to be 0.8 wt%.

Grafting of a silane in the presence of peroxide alters slightly the rheological properties of the starting EOC material, as shown in Fig. 1, because in the presence of free radicals, chain scission and recombination takes place. Recombination is the dominant mechanism for the polyethylene-based copolymers used in this work, thus a slight increase in viscosity compared to the base material is observed.

2.4. Morphology

The state of dispersion of the fillers was assessed by TEM imaging. Samples were compression molded using a Carver press at 150 °C and 10 MPa for 1 min. Ultra-thin sections were prepared using a Leica ultra microtome. The images obtained using a FEI

Table 1
EOC/nanosilica compositions in weight and volume percent.

Nanosilica content (wt%)	Vol% solid state	Vol% melt state
4	1.61	1.42
5	2.02	1.78
7	2.87	2.53
10	4.18	3.70
12	5.08	4.50

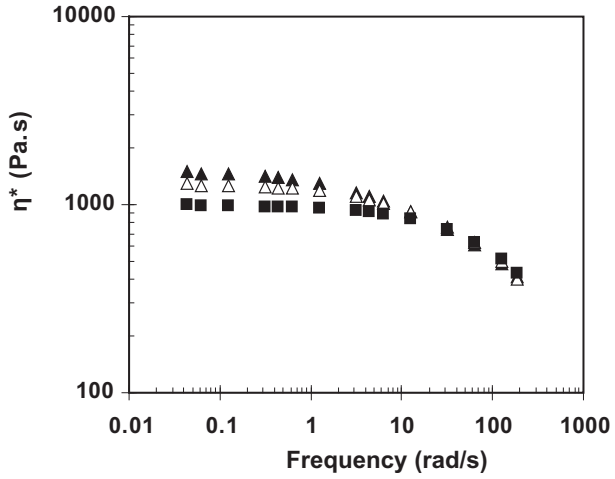

Fig. 1. Complex viscosity vs. frequency for unfilled EOCs at 190 °C. (■) EOC; (△) EOC-g-VTES; (▲) EOC-g-VTEOS.

Tecnai 20 instrument were converted into binary digital images according to the procedure described by Yatsuyanagi et al. [26]. Image analysis was subsequently performed using the SigmaScan Pro software to measure the area of the black colored phase corresponding to the silica particles and aggregates.

2.5. Rheological properties

Rheological characterization was carried out using a Reologica ViscoTech oscillatory rheometer equipped with 20 mm parallel plate fixtures under nitrogen purge, under a gap of 1 mm. Compression molded disks with a diameter of 20 mm were prepared using the Carver press, as described above.

Stress sweep experiments were carried out from 1 to 10^4 Pa at a frequency of 0.1 Hz and temperature of 200 °C. LVE frequency sweep experiments were performed in the dynamic oscillatory mode, under a constant strain of 10%, unless otherwise indicated. The elastic modulus (G'), loss modulus (G'') and complex viscosity (η^*) were measured as functions of the angular frequency (ω) at temperatures ranging from 80 °C to 200 °C. Time sweeps were performed at strains ranging between 1 and 10%, frequency of 0.1 rad/s and temperature of 190 °C.

Pre-shearing or annealing are commonly used to ensure a consistent shear history of silica suspensions prior to rheological evaluations [1,27]. However in this work since the primary concern was to correlate the rheological response to the structure of compression molded samples as evidenced by TEM imaging, no further shearing was applied to the compression molded disks used for rheology, unless otherwise specified.

The plateau modulus was estimated via the integration of the $G''(\omega)$ vs. ω method, which assumes that the distribution of the loss modulus with frequency is symmetric [28].

$$G_N^0 = \frac{4}{\pi}\int_{-\infty}^{\omega_{max}} G''(\omega)d\ln\omega \quad (1)$$

where ω_{max} is the frequency at which G'' reaches a maximum.

Whenever possible (at low filler loadings), time temperature superposition (TTS) from 80 °C to 200 °C was carried out to obtain the widest possible frequency range for this determination. At higher loadings, where TTS was not applicable, the measurements obtained at the lowest temperature (80 °C) were used for the estimation of the plateau modulus. The Generalized Maxwell model was employed to obtain the relaxation spectrum of the composites. A Fortran-based non-linear optimization program (UBCFIT), developed at the University of British Columbia, which follows the algorithm first developed by Baumgaertel at al. [29] and is based on the determination of the least number of (G_i, λ_i) parameters (Parsimonius spectrum) needed to provide a good fit was used. The Generalized Maxwell model was implemented to obtain the $G''(\omega)$ vs. ω function, which was then integrated in eq. (1).

2.6. Bound polymer determination

Chopped composites (1 g) were dissolved into 40 mL of toluene at 80 °C for 3 h to dissolve the polymer that was not bound to the filler. After cooling, the solution was subjected to centrifugal separation at 4000 rpm for 1 h. The supernatant was decanted and the gel was shaken with 30 mL of fresh toluene before being left to stand for 1 h. Centrifugal separation was repeated and the remaining gel containing the bound polymer and silica particles was dried under vacuum at 60 °C overnight. The amount of bound polymer was determined using a TA Instruments Q500 series thermogravimetric analysis instrument to heat samples under nitrogen atmosphere from 25 °C to 700 °C at a rate of 10 °C/min. Percent weight losses recorded for the SiO_2 and oct-SiO_2 particles, as well as for the plain and extracted composites, were used to calculate the amount of polymer bound to the filler.

2.7. Dynamic mechanical analysis

Dynamic mechanical properties were studied on rectangular 57.4 × 6.9 × 1 mm compression molded samples using a Rheometer Solid Analyzer RSA-II. The instrument was operated in the dual cantiliver configuration. The dynamic responses were tested from −100 to 20 °C at a frequency of 1 Hz and a heating ramp of 2 °C/min.

3. Results

3.1. Morphology

Fig. 2 displays the TEM images of the four different systems containing 7 wt% (Fig. 2(a1–d1)) and 12 wt% silica (Fig. 2(a2–d2)). Silica exists in an aggregated state with the size and shape of the aggregates varying slightly, depending on the type of matrix and particles used. Increasing the filler loading results in an increase in the area of the aggregates and a decrease in the inter-aggregate distance. At 12 wt% the composites appear to be almost interconnected, signifying that this composition is at the vicinity of the percolation threshold (Fig. 2(a2–d2)). Based on the images, nanosilicas dispersed within a polyolefin have a fractal structure, similar to that inferred for various colloidal and fumed nanosilica suspensions in liquid media. Fractal dimensions can be estimated based on image analysis of the TEM images, using the software developed by Sasaki et al. [30] According to this method, the fractal dimension d_f ranges between 2.2 and 2.4 for all the composites.

The results of the image analysis shown in Fig. 3 compare the size distribution of silica aggregates (Fig. 3(a)) and their relative contribution to the total area of the silica by size range (Fig. 3(b)), at a 7 wt% loading. It is obvious from these graphs that the size distribution of the aggregates (Fig. 3(a)) depends on the nature of the matrix and the silica treatment. Composites based on EOC-g-VTEOS have a higher fraction of isolated particles (area < 500 nm^2) and a smaller amount of large aggregates (area > 20,000 nm^2) than composites based on EOC-g-VTES, which display a higher fraction of large aggregates. Additionally the fraction of very large aggregates is reduced when oct-SiO_2 particles are used, as opposed to

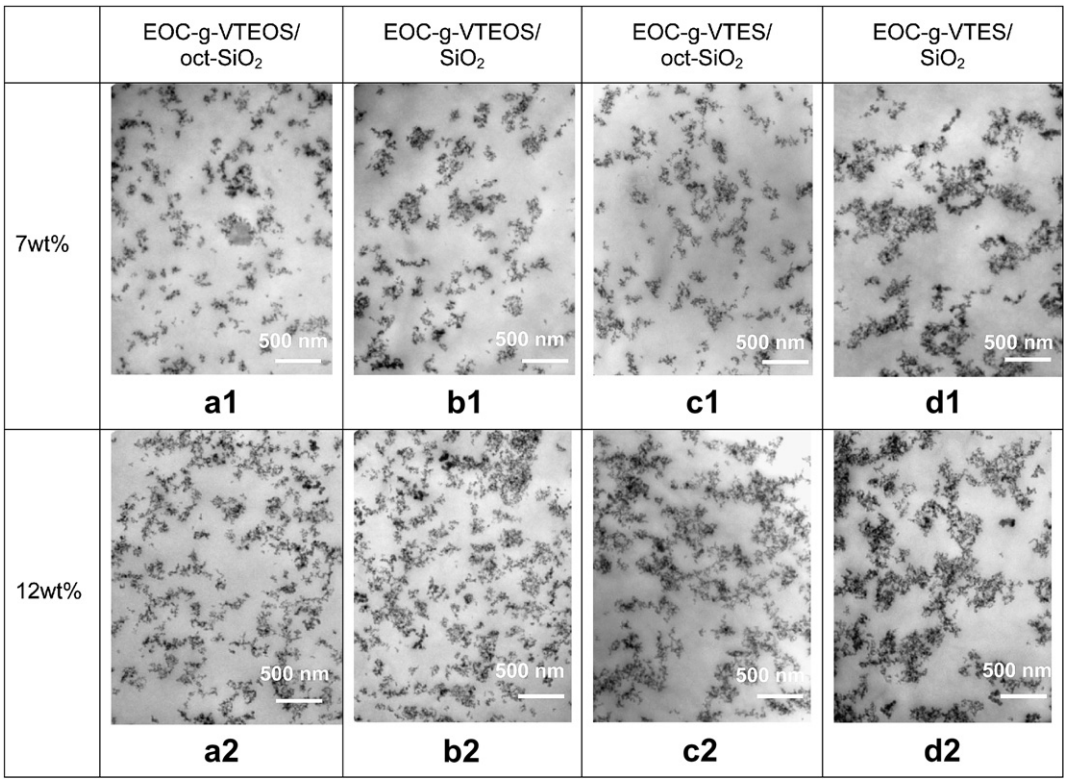

Fig. 2. TEM images of composites having different matrices: (a) EOC-g-VTEOS/oct-SiO_2; (b) EOC-g-VTEOS/SiO_2; (c) EOC-g-VTES/oct-SiO_2; (d) EOC-g-VTES/SiO_2. (a1–d1) 7 wt% silica, (a2–d2) 12 wt% silica. The scale bar represents 500 nm.

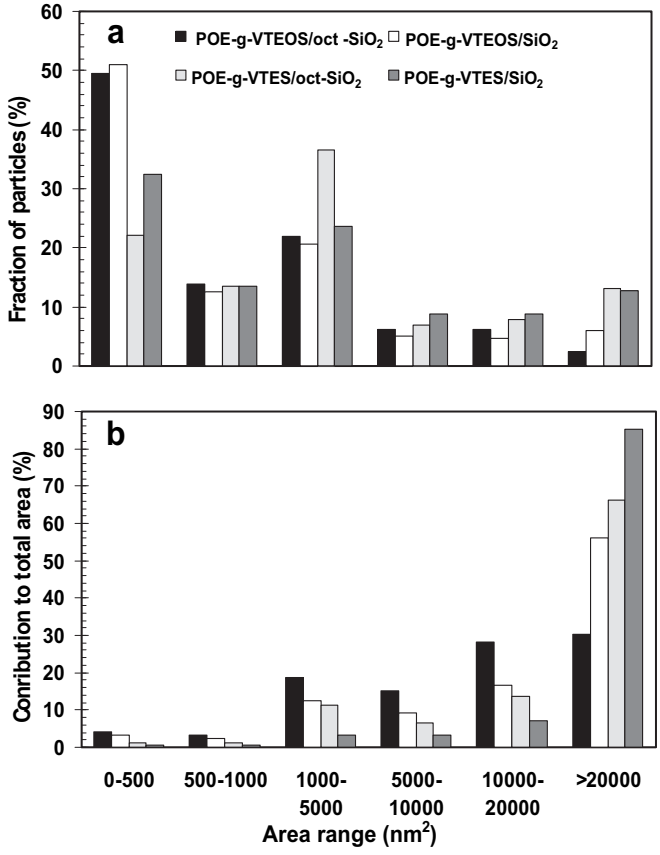

Fig. 3. (a) Silica aggregate size distribution and (b) % contribution to the total area per range of aggregate size. Silica loading is 7 wt%.

SiO_2 particles. Fig. 3(b) reveals that the vast majority of the silica particles can be found in large aggregates (e.g. 85% for EOC-g-VTES/SiO_2), except for EOC-g-VTEOS/oct-SiO_2 which shows a more balanced distribution. Apart from the size distribution of the aggregates, image analysis clearly confirms that their aspect ratio (defined as the smallest dimension over the largest dimension orthogonal to it) strongly depends on their size; the bigger the aggregate, the less spherical it is. Aspect ratios below 0.2 were found for the large aggregates having area above 20,000 nm^2, implying that they do not have a spherical shape; rather they appear to have a fractal structure [13].

The improved dispersion of the oct-SiO_2 particles within the polymer matrix is most likely due to the disruption of the hydrogen bonds between the silanol groups that cause aggregation. In the presence of the silane coating agent the specific component of the surface tension is lowered substantially, whereas the dispersive component becomes more significant, improving the affinity with the polyolefin matrix [31].

Dispersion is further facilitated by improving the stress transfer between polymer and fillers during compounding, thus breaking the aggregates apart. This can be achieved by establishing stronger polymer/filler interactions. The difference between VTEOS and VTES lies in the presence of the ethoxy groups in VTEOS instead of the alkyl groups in VTES. The hydroxyl groups present at the surface of the particles can react with the ethoxy groups of VTEOS through a hydrolysis reaction [23], thus establishing strong interfacial interactions between the polymer and fillers, according to Scheme 1. However, in the absence of the ethoxy group in VTES, this reaction cannot take place.

The effectiveness of this functionalization approach is seen by comparing Fig. 2(b1) with (d1), as well as (b2) with (d2). In the presence of covalent bonds when the EOC-g-VTEOS matrix is used, the dispersion of unmodified SiO_2 particles appears substantially

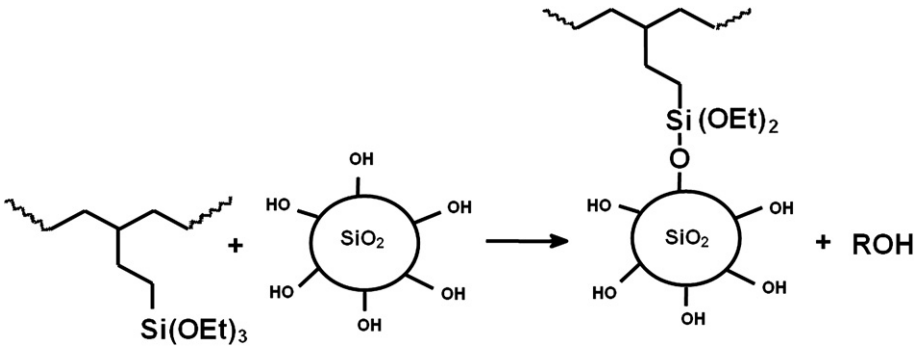

Scheme 1. Schematic illustration of the hydrolysis reaction between the silanol groups located at the surface of SiO_2, with the VTEOS grafts contained in the polyolefin matrix.

improved. The EOC-g-VTEOS/oct-SiO_2 composite (Fig. 2(a1) and (a2)) contains the lowest fraction of large aggregates compared to the rest of the composites (see also Fig. 3). This composite has benefited from particle modification, which reduces the filler/filler interactions, while still maintaining some capacity for polymer/filler interactions through covalent bonding, since the hydroxyl groups are only partially replaced by the silane coating agent.

Based on the above results, filler dispersion is obviously affected by the presence and extent of polymer/filler interactions. Bound polymer characterizations are frequently used in rubber technology as a means to quantify polymer/filler interactions [32]. This technique has been applied to the composites under consideration in this work, as described below.

3.2. Bound polymer characterizations and effective volume

As shown in Table 2 the amount of polymer that is bound to the filler is higher in the EOC-g-VTEOS-based composites compared to the ones having EOC-g-VTES as the matrix. SiO_2 particles have the most potential for covalent bond formation between the silanol groups and the VTEOS grafts and therefore have the high amount of bound polymer. The presence of bound polymer in EOC-g-VTES-based composites may be attributed to residual polymer that has been physically adsorbed or trapped within the large particle aggregates [12,26].

The presence of an immobilized "bound" polymer layer has been related to substantial increases in the rheological properties of filled polymers. The concept of an "effective volume fraction" which takes into account not only the volume occupied by the particles, but also that of the rigid shell surrounding them, has been used to explain this increase. Assuming an idealized case of spherical silica particles of density 2.2 g cm^{-3} and diameter of 12 nm surrounded by a bound polymer shell of density 0.864 g cm^{-3}, a shell thickness can be estimated from this data and is also shown in Table 2.

Table 2
Amount of bound polymer and estimated thickness of polymeric shell surrounding the particles, for composites containing 7 wt% silica.

	EOC-g-VTEOS/oct-SiO_2	EOC-g-VTEOS/SiO_2	EOC-g-VTES/oct-SiO_2	EOC-g-VTES/SiO_2
Bound polymer (wt%)	7.0	10.2	3.5	6.1
Bound polymer per mass of silica	1.0	1.5	0.5	0.9
Shell thickness estimated from bound polymer (nm)	2.9	3.8	1.7	2.7
Shell thickness estimated through eqs. (2) and (4)(nm)[a]	2.5	2.9	N/A	N/A

[a] Using the Heinrich and Kluppel equation and least squares method.

In addition to the calculation of the thickness, or volume of the immobilized shell around silica particles, an effective particle volume fraction can be estimated from values of the plateau modulus by using the modified Guth–Smallwood equation [33] proposed by White and Crowder [34].

$$G_N(\phi_e) = G_N(0)\cdot\left(1 + 2.5\phi_e + 14.1\phi_e^2\right) \quad (2)$$

where G_N is the plateau modulus and ϕ_e the effective volume fraction. White and Crowder proposed an expression to estimate the effective volume fraction based on the average particle diameter d and the shell thickness Δ.

$$\phi_e = \phi + \left(\frac{6\phi}{d}\right)\Delta \quad (3)$$

Heinrich and Kluppel [13] proposed an alternative expression, shown in eq. (4) to take into account the fact that particles are interconnected and therefore the shell does not exist at the particle–particle intersection.

$$\phi_e = \frac{(d+2\Delta)^3 - 6d\Delta^2}{d^3}\phi \quad (4)$$

where d is the average particle diameter (12 nm in our case) and Δ is the shell thickness, provided that $\Delta << d$ [13]. Eq. (2), in combination with eq. (4), was used to fit the experimental data of plateau modulus vs. volume fraction. A representative fit is shown in Fig. 4 for the EOC-g-VTEOS/oct-SiO_2 composite. The fitted values obtained for EOC-g-VTEOS/oct-SiO_2 and EOC-g-VTEOS/SiO_2 are shown in Table 2.

Values for the EOC-g-VTES composites are not presented here because of the uncertainties in the rheological characterization leading to the estimation of the plateau modulus due to pronounced time-dependent effects, as explained later in Section 3.3. Although the values of the shell thickness are lower than the ones estimated through the bound rubber characterization (which were based on the idealized case of spherical silica particles), the trends are the same and verify that the EOC-g-VTEOS/SiO_2 composite has more bound rubber, because the unmodified SiO_2 has a higher number of free silanol groups that are able to engage in covalent bonding with the matrix. Overall the values of the shell thickness are in the same order of magnitude and agree with literature reports [27,32].

It should be noted that the effective volume fraction estimated using this approach is about 2.5–3 times the real volume fraction, as shown in Fig. 5. This agrees with the values obtained by Zhang and Archer [27] and supports the hypothesis of the existence of

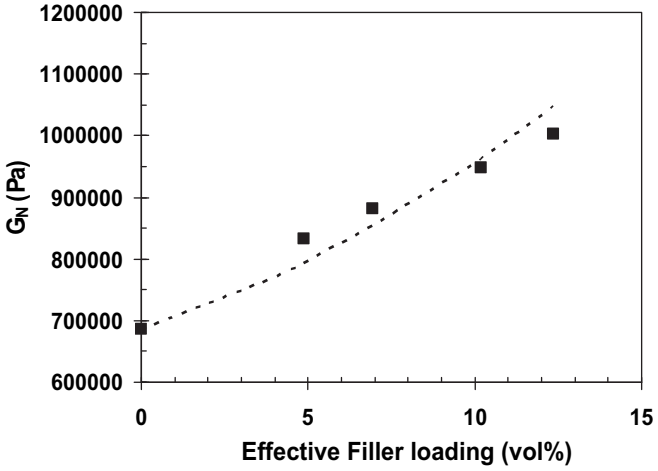

Fig. 4. Fit of the experimental values of the plateau modulus (squares) of the EOC-g-VTEOS/oct-SiO_2 composite using the modified Guth–Smallwood equation (dashed line) at a fitted value of the shell thickness ($\Delta = 2.5$ nm).

a bound polymer layer surrounding the silica aggregates that causes an enhanced hydrodynamic effect. The effective volume fraction is higher for the EOC-g-VTEOS/SiO_2 composite, consistently with its larger shell thickness.

3.3. Shear oscillatory rheology

3.3.1. Frequency sweeps

Frequency sweeps demonstrate deviations from terminal flow behaviour at filler loadings above 5–7 wt% (Fig. 6), suggesting that the motion of the polymer chains becomes restricted above this filler loading. The deviation can be better seen from the insets in Fig. 6, which summarize the normalized moduli as a function of filler loading. It should be noted that the emergence of a low-frequency plateau is only seen at the highest filler loadings. For all other compositions the values of the loss tangent, tanδ, remain higher than one, indicating a viscoelastic-liquid response, which is consistent with the fact that these composites are below the percolation threshold, as evidenced by TEM (Fig. 2).

Fig. 7 shows a representative frequency sweep for the neat polymer and the EOC-g-VTEOS/SiO_2 composite. In contrast to the simple dynamics and terminal flow behaviour demonstrated by the

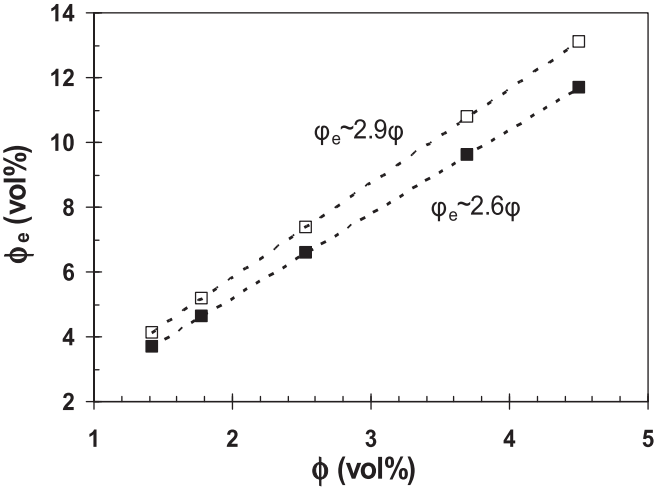

Fig. 5. Effective filler content, in volume percent, φ_e vs. actual filler content, in volume percent, φ. (■) EOC-g-VTEOS/oct-SiO_2; (□) EOC-g-VTEOS/SiO_2.

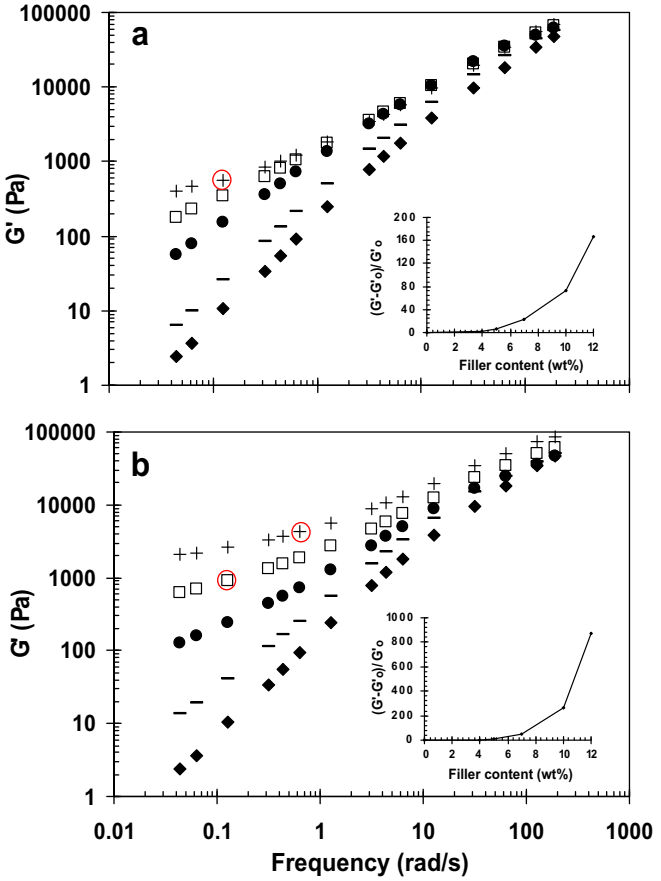

Fig. 6. Frequency dependence of the storage modulus (G') for (a) EOC-g-VTEOS/oct-SiO_2 and (b) EOC-g-VTEOS/SiO_2 composites at 190 °C. SiO_2 or oct-SiO_2 content: (◆) 0wt%; (–) 4 wt%; (•) 7 wt%; (□) 10 wt%; (+) 12 wt%. Cross-over points of storage and loss moduli are circled. Insets show the normalized moduli with respect to the matrix modulus, G'_0.

matrix, the composites exhibit a cross-over at low frequencies at the highest filler loadings, indicating a viscoelastic solid-like response. These complex frequency and volume fraction dependencies are attributed to the interaction between the filler structure and the viscoelastic response of the matrix [35]. Both the frequency and the modulus at which this cross-over appears increase with filler loading, as shown in Fig. 6.

Fig. 8 summarizes the G'_0 vs. volume fraction dependency at the lowest accessible experimental frequency, $G'_0 = G'(\omega = 0.04$ rad/s). A smooth scaling relationship of $G'_0 \sim \varphi^m$ between G'_0 and filler loading is seen, with the exponent values for the EOC-g-VTEOS based composites shown in Table 3. For the EOC-g-VTEOS/oct-SiO_2 composites a scaling relation of $G'_0 \sim \varphi^{3.5}$ is obtained. This is strikingly similar to the reports by Zhu et al. on polybutadiene nanosilica suspensions and representative of reinforcement due to the formation of a fractal structure [13,14]. The dependency is sharper for the EOC-g-VTEOS/SiO_2 composite, presumably because of an enhanced hydrodynamic effect.

Several models have been proposed to describe the fractal structure arising from colloidal particle aggregation processes. Piau et al. considered non-fluctuating semidilute fractal objects, and showed that the elastic modulus scales with the volume fraction according to a power-law, $G'_0 \sim \varphi^m$, where the exponent m contains the fractal dimension, d_f [6].

$$G_o' \sim \phi^{\frac{5}{3-d_f}} \quad (5)$$

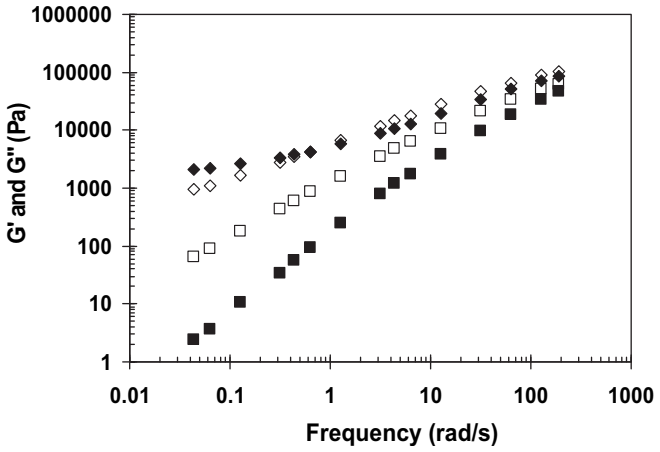

Fig. 7. Frequency sweep at 190 °C of EOC-g-VTEOS (squares) and EOC-g-VTEOS/12 wt% SiO_2 (diamonds). G' (full symbols) and G'' (empty symbols).

Values of the fractal dimension d_f can be experimentally obtained either by image analysis [11], light-scattering experiments [6] or indirectly by rheology [36]. The values of the fractal dimension obtained through eq. (5) and reported in Table 3 are very close to literature reports. For example Piau et al. reported an exponent of $m = 4.2 \pm 0.8$ and a corresponding fractal dimension of $d_f = 1.8 \pm 0.2$ for PDMS/SiO_2 gels. A lower value of d_f is obtained for EOC-g-VTEOS/oct-SiO_2 composites. This value is consistent with the predictions of the cluster–cluster aggregation (CCA) model, which is based on the concept that particles can fluctuate around their mean position to eventually lead to a space-filling configuration of fractal CCA-clusters [13]. The CCA model predicts $m \approx 3.5$ and $d_f \approx 1.8$, which is very similar to our results for the EOC-g-VTEOS/oct-SiO_2 composite.

These results demonstrate that the magnitude of the modulus at low frequencies and the corresponding scaling factors and fractal dimensions vary depending on the type of matrix and nature of filler treatment. Further insight on the effect of polymer/filler interactions on the rheological properties is provided through time sweeps and strain-sweeps, as discussed below.

3.3.2. Time sweeps

It is well known that suspensions of fumed silica experience microstructural rearrangements during shear, leading to flocculation and formation of particle aggregates [1,27]. Functionalized polyolefins that are commonly used as nanocomposite matrices are also prone to time-dependent effects, because of the propensity for functional group associations [37].

Table 3
Values of exponent, m, and fractal dimension, d_f (eq. (5)) obtained by curve fitting the G'_0 vs. volume fraction data. The reported values include the 95% confidence intervals.

	EOC-g-VTEOS/oct-SiO_2	EOC-g-VTEOS/SiO_2
m	3.5 ± 0.1	4.4 ± 0.2
d_f	1.6 ± 0.04	1.9 ± 0.05

Time-dependency was noted at filler loadings above 5 wt%, signifying that a certain amount of filler is required in order to observe a rearrangement and a corresponding increase in modulus, as pointed out previously by Romeo et al. [35]. A pronounced increase in storage modulus was seen for the EOC-g-VTES-based composites, as shown in Fig. 9, suggesting that the silica particles have the propensity to associate and form aggregates, when exposed to low strains during the time sweeps. This was the reason why these composites were excluded from the prior analysis of the frequency sweeps. The significantly higher starting elastic modulus values seen for the EOC-g-VTES/SiO_2 composite in Fig. 9 are most likely related to the higher state of aggregation of the filler in this particular matrix.

The dramatic increase seen in these composites implies that the free silanol groups existing on the silica surface maintain their capability to associate through hydrogen bonding under the low strains imposed during the time sweep experiments, thereby leading to strong filler/filler interactions and thus aggregation. The situation changes when the VTEOS-based matrix is used, since the silanol groups are now able to form covalent bonds with the ethoxysilane functionality. This limits their capacity to associate with each other and form aggregates, leading to a steady rheological response, presumably attributed to a more stable morphology.

It is also noteworthy that these composites are very sensitive to pre-shearing, indicating that the flocculated clusters of silica can be broken down by relatively high levels of shearing. Furthermore the rate and extent of modulus recovery following pre-shearing depends on the strain level imposed during time sweeps, as shown in Fig. 10. Higher levels of strain during the time sweeps result in a breakdown of the structure, which counteracts the continuous

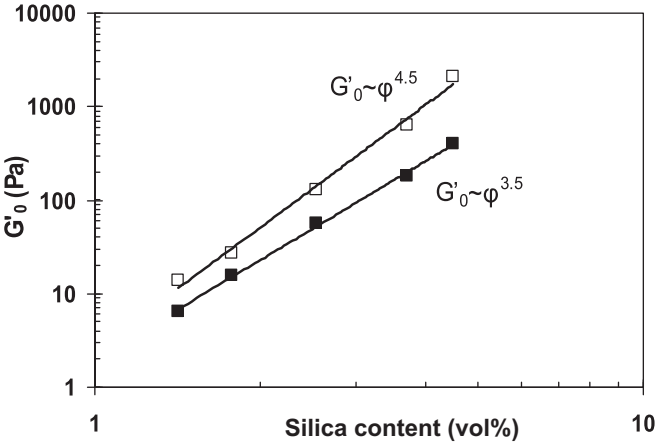

Fig. 8. Elastic modulus at $\omega = 0.04$ rad/s as a function of the silica loading. (■) EOC-g-VTEOS/oct-SiO_2; (□) EOC-g-VTEOS/SiO_2. Lines indicate exponential model fit.

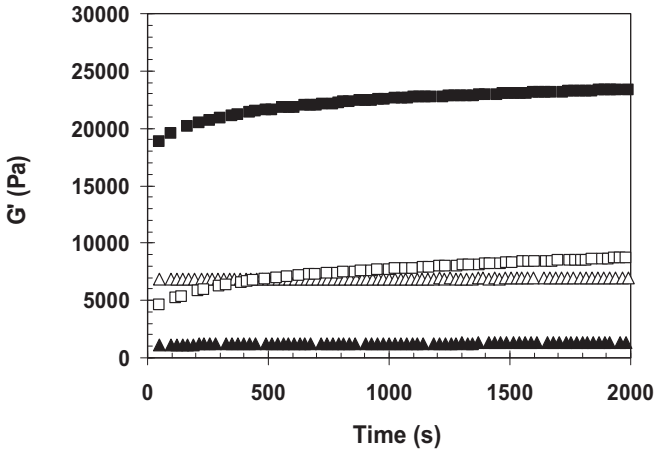

Fig. 9. Storage modulus G' as a function of time, at 190 °C under a 2% strain and 0.1 Hz frequency. Silica content is 12 wt%. (▲) EOC-g-VTEOS/oct-SiO_2; (△) EOC-g-VTEOS/SiO_2. (□) EOC-g-VTES/oct-SiO_2; (■) EOC-g-VTES/SiO_2.

buildup, leading to lower values of the modulus and the appearance of a plateau.

3.3.3. Stress sweeps

A pronounced difference in strain dependence between the EOC-g-VTEOS and the EOC-g-VTES-based composites at filler loadings above 7 wt% is revealed from the stress sweeps, shown in Fig. 11. The critical strain, γ_c, for the onset of non-linearity is significantly lower for the EOC-g-VTES compared to the EOC-g-VTEOS-based composites, with the latter being more strain resistant (Fig. 11). Given that a continuous "filler network" does not exist at the loadings used in the present work, the drop of γ_c is most likely attributed to the breakdown of the nanosilica aggregates during the stress-sweep [7,9,12,36,38]. The EOC-g-VTES/oct-SiO_2 composite shows a very strong strain dependence; the elastic modulus curve increases at moderate strains, and subsequently decreases. The initial increase may be due to "strain-induced" aggregation. This is in agreement with the findings from the time sweep reported previously, where this particular composite seemed to be prone to aggregation.

The critical strain $-\gamma_c-$ for the onset of non-linearity shifts to lower strain values upon increasing silica concentration. This is shown in Fig. 12, which summarizes the critical strain, estimated as the strain reached when the modulus is equal to 95% of the plateau modulus as a function of the silica loading [39]. Given the absence of a well-defined linear region for EOC-g-VTES/oct-SiO_2, data are not shown for this particular composite. The data can be fitted using a power-law scaling relation [9,16].

$$\gamma_c \propto \phi^{-\nu} \tag{6}$$

where ν is a parameter, which according to the literature ranges in value from 0.7 to 4.0 and depends on the interparticle forces [16]. The EOC-g-VTES-based composites are significantly more sensitive to strain, resulting in an exponent of 1.6 ± 0.2 for EOC-g-VTES/SiO_2. On the contrary the EOC-g-VTEOS-based composites are more resistant to strain, with lower exponents, 0.5 ± 0.05 and 0.3 ± 0.04 respectively for SiO_2 and oct-SiO_2 particles.

The critical strain, γ_c can be related to the cohesive energy density, E_c, needed to break the filler structure, according to eq. (6) [40].

$$E_c = \frac{1}{2}\gamma_c^2 G'_{\text{plateau}} \tag{7}$$

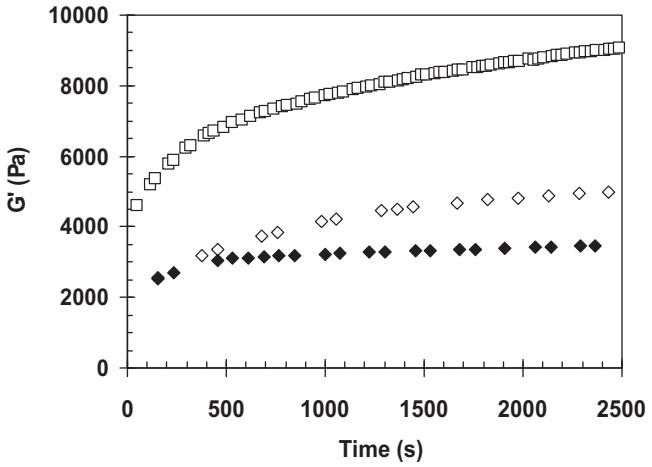

Fig. 10. Storage modulus as a function of time for POE-g-VTES/oct-SiO_2 at 190 °C and 0.1 Hz frequency: (□) no preshear; (◇) pre-sheared at 1000 Pa for 100 s, strain of 1% during time sweep; (◆) pre-sheared at 1000 Pa for 100 s, strain of 10% during time sweep.

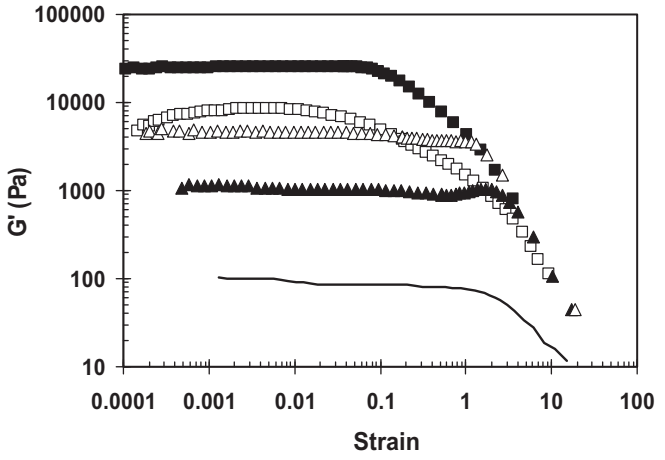

Fig. 11. Storage modulus vs. strain at 200 °C, 0.1 Hz at a silica loading of 12 wt%; (▲) EOC-g-VTEOS/oct-SiO_2; (△) EOC-g-VTEOS/SiO_2. (□) EOC-g-VTES/oct-SiO_2; (■) EOC-g-VTES/SiO_2; The solid line represents the unfilled EOC-g-VTEOS matrix.

Application of this equation to our data shows that for EOC-g-VTES/SiO_2 the work required to breakdown the structure remains around 10 J m^{-3} irrespective of the filler loading, as opposed to EOC-g-VTEOS-based composites in which E_c increases with filler loading, reaching values above 50 J m^{-3} at high loadings. This confirms that the structure of the EOC-g-VTEOS composites, where covalent bonds are present, is much more strain resistant.

The presence of a small peak in the elastic modulus vs. strain curves of the EOC-g-VTEOS composites at very large strains (Fig. 11), right beyond the strain where the transition to non-linear behaviour occurs in the pure polymer is also noteworthy. To our knowledge this has never been reported before, except from a similar observation by Cassagnau [41] in silica-filled EVA/xylene mixtures. One possible explanation is stress-induced debonding of the polymer chains that are bound to the filler surface through covalent bonding.

3.4. Dynamic mechanical analysis

Fig. 13(a) and (b) present the storage and loss moduli as functions of temperature, obtained from the DMA measurements. For clarity, only the composites containing oct-SiO_2 are shown here.

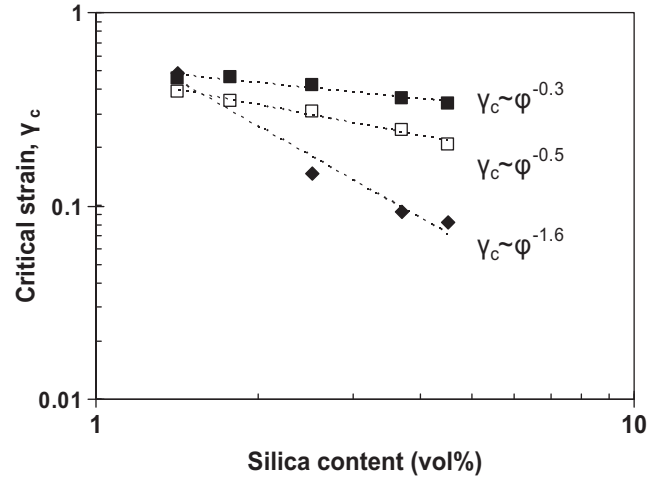

Fig. 12. Critical strain γ_c vs. silica content: (■) EOC-g-VTEOS/oct-SiO_2; (□) EOC-g-VTEOS/SiO_2; (◆) EOC-g-VTES/SiO_2; Lines indicate exponential model fit.

Fig. 13(a) shows that although both the neat polymers and the composites have similar values of the storage moduli at temperatures below the glass transition, their behavior at temperatures around and above the glass transition differs, with the EOC-g-VTEOS-based composite showing a higher value of the elastic modulus and a more significant enhancement with respect to the neat polymer. Similarly, as Fig. 13(b) shows, the area under the loss modulus vs. temperature curve is higher for the EOC-g-VTEOS based composite, suggesting that more energy is dissipated when the glass transition temperature is reached, at about −50 °C.

On the contrary the curves corresponding to the EOC-g-VTES composite are very similar to the response of the neat polymer, suggesting a minimal effect of the filler. The type of filler (modified vs. unmodified) did not affect the results, implying that the most important factor is the matrix functionalization. It can be suggested therefore that the dynamic elastic and loss moduli are affected only when polymer/filler interactions are present. Furthermore, these figures suggest a very slight increase in the glass transition temperature, T_g, for the EOC-g-VTEOS composites, presumably because the motion of macromolecules at the vicinity of the nanoparticles is hindered in the presence of chain entanglements and polymer/filler interactions, therefore leading to a higher T_g [18].

4. Discussion

The rheology of filled thermoplastics is influenced by both the presence of nanofillers as well as their state of dispersion. The latter further depends on the extent of filler/filler and polymer/filler interactions. Given these complex interrelations, it is has been very challenging in the literature to differentiate between the effects of filler dispersion and polymer/filler interactions. In this work, by using two different matrices and two types of silica particles, we were able to gain some insight on the dependence of the composite structure and the various rheological functions on the filler/filler and polymer/filler interactions.

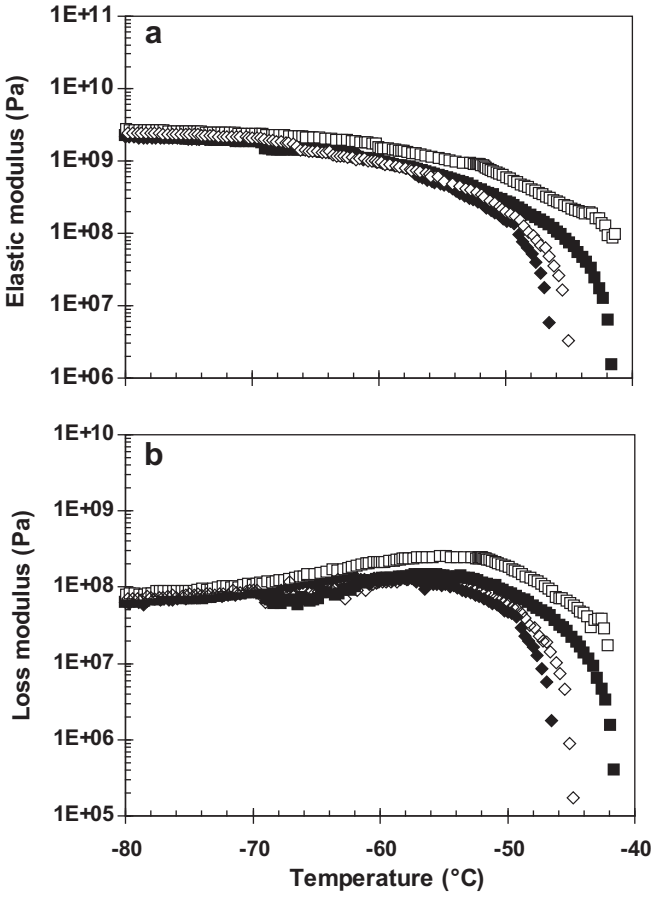

Fig. 13. DMA curves at 1 Hz for composites containing 7 wt% silica: (a) Storage modulus and (b) Storage modulus; (■) EOC-g-VTEOS; (□) EOC-g-VTEOS/oct-SiO_2; (◆) EOC-g-VTES; (◆) EOC-g-VTES/oct-SiO_2; Silica content is 7 wt%.

The different types of filler/filler and polymer/filler interactions are reflected in the different states of dispersion (Figs. 2 and 3), as well as in the exponents of the $G' \sim \varphi^m$ scaling relation (Table 3). Enhanced polymer/filler interactions that are mainly attributed to covalent bonding between the surface silanol groups and the functional grafts present in the polymer matrix have an impact on the state of dispersion of the composites. As the results of image analysis showed, composites based on EOC-g-VTEOS present a lower state of aggregation compared to EOC-g-VTES-based composites, regardless of the extent of filler/filler interactions (i.e. type of particle used). Overall, EOC-g-VTEOS/oct-SiO_2 displays the finest dispersion because it combines both a lower degree of filler/filler interactions and stronger polymer/filler interactions.

The increases seen in the viscoelastic properties as a function of filler loading, are obviously attributed first of all to the hydrodynamic effect caused by the nanoparticles, and at higher loadings (above 5 wt%, or 2 vol%) to the propensity of the silica particles to aggregate and form flocculated clusters, leading to a fractal structure, with dimensions consistent to the predictions of the CCA model.

A volume fraction of $\varphi_c = 0.05$ is generally acknowledged as the critical volume fraction beyond which a network consisting of overlapping clusters is formed, as predicted by Buscall et al. [8] and Huber and Vilgis [14]. Belowφ_c the elastic modulus varies linearly with volume fraction, whereas above φ_c universal behaviour with scalings of $G' \sim \varphi^m$ is reported. Interestingly, even though all our composites are below the critical volume fraction of $\varphi_c = 0.05$, they obey the $G' \sim \varphi^m$ scaling behaviour (see Fig. 8 and Table 3), which at first glance is inconsistent. However, the effective volume fractions, which take into account the presence of bound polymer, are actually around three times the actual volume fractions, as implied by Fig. 5, and may thus account for the observed rheological behaviour.

Measurements in the LVE region are inherently influenced by the degree of dispersion, therefore provide only indirect evidence of the existence of covalent bonding resulting in strong polymer/filler interactions. In this work, the latter became more evident through the time sweeps, stress-sweeps and DMA analysis. Covalently bridging the polymer chains and the nanoparticles in the EOC-g-VTEOS based composites resulted in “anchoring” of the filler to the polymer chains, thus preventing rearrangements and further aggregation of the particles during time sweeps (Fig. 9), in contrast with the EOC-g-VTES composites where covalent bonding was absent. The more stable structure of the EOC-g-VTEOS based composites was also evident from the stress-sweep experiments, where they appeared to be very strain resistant, with critical strain values that were an order of magnitude higher and a cohesive energy density 5 times higher than that of the VTES-based counterparts. The onset of non-linearity for these composites does not seem to be attributed to the breakdown of a filler network, as it has been widely suggested in the past [9,10,36,42–44], but rather depends on the type of interfacial interactions between polymer and filler. It should be noted that the EOC-g-VTEOS/oct-SiO_2 composites were the most strain resistant. Although silica particles have been modified, it should be noted that the coating is only partial, leaving a lot of silanol groups available for the reaction. These composites therefore benefit from both the absence of big aggregates, and the presence of covalent bonding. Finally, DMA measurements revealed that the energy

dissipated during the glass transition was significantly higher in the EOC-g-VTEOS based composites, and the elastic modulus above the transition was higher.

5. Conclusions

Grafting reactive and non-reactive silanes onto an EOC matrix enabled the differentiation between two different types of composites, based on the presence or absence of polymer/filler interactions due to covalent bonding. The amount of bound polymer was higher when VTEOS, which is able to form covalent bonds with the hydroxyl groups of silica, was grafted onto the EOC matrix. Both particle modification and grafting of VTEOS on the EOC matrix contributed to a finer dispersion of the nanoparticles, as revealed through TEM imaging.

The values of the moduli at low frequencies scaled with the volume fraction according to a power-law relation, which is consistent with the presence of a fractal structure. Given that the composites were below the percolation threshold, this observation is attributed to the higher effective volume of the filler particles, in the presence of bound polymer.

Time-sweep experiments showed that the composites were prone to aggregation, in the absence of chemical interactions between filler and hosting polymer. Stress-sweeps revealed that VTEOS grafted composites were more capable of enduring high strains without significant network disruption, as their critical strains were much higher compared to VTES grafted composites. This behaviour was attributed to the presence of polymer/filler interactions that create linkages between the hosting polymer chains and the nanoparticles. Differences were also detected in the solid state DMA evaluations, which showed that a higher amount of energy is dissipated at the glass transition temperature when the VTEOS-based composites were used.

Acknowledgements

This research has been supported by the Natural Sciences and Engineering Research Council of Canada (NSERC), Discovery and Strategic Grant programs. The authors would like to thank Evonic Industries for donating the nanosilica samples used in this work.

References

[1] Raghavan SR, Khan SA. J Rheol 1995;39(6):1311–25.
[2] Khan SA, Zoeller NJ. J Rheol 1993;37(6):1225–35.
[3] Kraus G. Reinforcement of elastomers. New York: Interscience Publishers; 1965.
[4] Zou H, Wu S, Shen J. Chem Rev 2008;108(9):3893–957. doi:10.1021/cr068035q.
[5] de Gennes PG. Scaling concepts in polymer physics. Ithaca, New York: Cornell University Press; 1979.
[6] Piau JM, Dorget M, Palierne JF. J Rheol 1999;43(2):305–14.
[7] Galindo-Rosales FJ, Rubio-Hernandez FJ, Velazquez-Navarro JF. Rheol Acta 2009;48(6):699–708. doi:10.1007/s00397-009-0367-7.
[8] Buscall R, Mills PDA, Goodwin JW, Lawson DW. J Chem Soc Faraday Trans 1: Phys Chem Condensed Phases 1988;84(12):4249–60. doi:10.1039/F19888404249.
[9] Yziquel F, Carreau PJ, Tanguy PA. Rheol Acta 1999;38(1):14–25.
[10] Rueb CJ, Zukoski CF. J Rheol 1997;41(2):197–218.
[11] Chakraborti RK, Atkinson JF, Van Benschoten JE. Environ Sci Technol 2000;34(18):3969–76. doi:10.1021/es990818o.
[12] Wang MJ. Rubber Chem Technol 1998;71(3):520–89.
[13] Heinrich G, Kluppel M. Recent advances in the theory of filler networking in elastomers. In: Anonymous filled elastomers drug delivery systems. Berlin: Heidelberg; 2002. p. 1–44.
[14] Huber GA, Vilgis T. Macromolecules 2002;35(24):9204–10. doi:10.1021/ma0208887.
[15] Shang SW, Williams JW, Soderholm KJM. J Mater Sci 1995;30(17):4323–34.
[16] Cassagnau P. Polymer 2008;49(9):2183–96. doi:10.1016/j.polymer.2007.12.035.
[17] Aranguren MI, Mora E, Degroot JV, Macosko CW. J Rheol 1992;36(6):1165–82.
[18] Wu C, Liao H. J Appl Polym Sci 2003;88(4):966–72. doi:10.1002/app.11725.
[19] Barus S, Zanetti M, Lazzari M, Costa L. Polymer 2009;50(12):2595–600. doi:10.1016/j.polymer.2009.04.012.
[20] Rong MZ, Zhang MQ, Ruan WH. Mater Sci Technol 2006;22(7):787–96. doi:10.1179/174328406X101247.
[21] Bansal A, Yang H, Li C, Benicewicz BC, Kumar SK, Schadler LS. J Polym Sci B Polym Phys 2006;44(20):2944–50. doi:10.1002/polb.20926.
[22] Taniguchi Y, Shirai K, Saitoh H, Yamauchi T, Tsubokawa N. Polymer 2005;46(8):2541–7. doi:10.1016/j.polymer.2005.02.016.
[23] Bailly M, Kontopoulou M. Polymer 2009;50(11):2472–80.
[24] Sengupta SS, Parent JS. Polym Eng Sci 2006;46(4):480–5. doi:10.1002/pen.20500.
[25] Sato Y, Hashiguchi H, Inohara K, Takishima S, Masuoka H. Fluid Phase Equilib 2007;257(2):124–30. doi:10.1016/j.fluid.2007.01.013.
[26] Yatsuyanagi F, Suzuki N, Ito M, Kaidou H. Polymer 2001;42(23):9523–9. doi:10.1016/S0032-3861(01)00472-4.
[27] Zhang Q, Archer LA. Langmuir 2002;18(26):10435–42. doi:10.1021/la026338j.
[28] Liu C, He J, Ruymbeke Ev, Keunings R, Bailly C. Polymer 2006;47(13):4461–79. doi:10.1016/j.polymer.2006.04.054.
[29] Baumgaertel M, Winter HH. Rheol Acta 1989;28(6):511–9.
[30] Sasaki H, Shibata S, Hatanaka T. Bull Natl Grassl Res Inst 1994;49:17–24.
[31] Elias L, Fenouillot F, Majesté JC, Alcouffe P, Cassagnau P. Polymer 2008;49(20):4378–85. doi:10.1016/j.polymer.2008.07.018.
[32] Leblanc JL. Prog Polym Sci 2002;27(4):627–87.
[33] Smallwood HM. J Appl Phys 1944;15(11):758–66.
[34] White JL, Crowder JW. J Appl Polym Sci 1974;18(4):1013–38.
[35] Romeo G, Filippone G, Fernández-Nieves A, Russo P, Acierno D. Rheol Acta 2008;47(9):989–97. doi:10.1007/s00397-008-0291-2.
[36] Paquien JN, Galy J, Gerard JF, Pouchelon A. Colloid Surf A-Physicochem Eng Asp 2005;260(1–3):165–72.
[37] Lee JA, Kontopoulou M, Parent JS. Polymer 2004;45(19):6595–600. doi:10.1016/j.polymer.2004.07.017.
[38] Cassagnau P, Mélis F. Polymer 2003;44(21):6607–15. doi:10.1016/S0032-3861(03)00689-X.
[39] Abbasi S, Carreau P, Derdouri A, Moan M. Rheol Acta 2009;48(9):943–59. doi:10.1007/s00397-009-0375-7.
[40] Bossard F, Moan M, Aubry T. J Rheol 2007;51(6):1253–70. doi:10.1122/1.2790023.
[41] Cassagnau P. Polymer 2003;44(8):2455–62. doi:10.1016/S0032-3861(03)00094-6.
[42] Zhu Z, Thompson T, Wang S, Meerwall EDV, Halasa A. Macromolecules 2005;38(21):8816–24. doi:10.1021/ma050922s.
[43] Clement F, Bokobza L, Monnerie L. Rubber Chem Technol 2005;78(2):211–31.
[44] Ramier J, Gauthier C, Chazeau L, Stelandre L, Guy L. J Polym Sci Pt B-Polym Phys 2007;45(3):286–98. doi:10.1002/polb.21033.